



# Control of CCND1 ubiquitylation by the catalytic SAGA subunit USP22 is essential for cell cycle progression through G1 in cancer cells

Victoria J. Gennaro<sup>a</sup>, Timothy J. Stanek<sup>a</sup>, Amy R. Peck<sup>b</sup>, Yunguang Sun<sup>b</sup>, Feng Wang<sup>c</sup>, Shuo Qie<sup>d</sup>, Karen E. Knudsen<sup>e</sup>, Hallgeir Rui<sup>b</sup>, Tauseef Butt<sup>c</sup>, J. Alan Diehl<sup>d</sup>, and Steven B. McMahon<sup>a,1</sup>

<sup>a</sup>Department of Biochemistry and Molecular Biology, Sidney Kimmel Medical College, Thomas Jefferson University, Philadelphia, PA 19107; <sup>b</sup>Department of Pathology, Medical College of Wisconsin, Milwaukee, WI 53226; <sup>c</sup>Progenra, Inc., Malvern, PA 19355; <sup>d</sup>Department of Biochemistry and Molecular Biology, Medical University of South Carolina, Charleston, SC 29425; and <sup>e</sup>Department of Cancer Biology, Sidney Kimmel Medical College and Sidney Kimmel Cancer Center, Thomas Jefferson University, Philadelphia, PA 19107

Edited by Charles J. Sherr, HHMI and St. Jude Children's Research Hospital, Memphis, TN, and approved August 10, 2018 (received for review May 8, 2018)

**Overexpression of the deubiquitylase ubiquitin-specific peptidase 22 (USP22) is a marker of aggressive cancer phenotypes like metastasis, therapy resistance, and poor survival. Functionally, this overexpression of USP22 actively contributes to tumorigenesis, as USP22 depletion blocks cancer cell cycle progression in vitro, and inhibits tumor progression in animal models of lung, breast, bladder, ovarian, and liver cancer, among others. Current models suggest that USP22 mediates these biological effects via its role in epigenetic regulation as a subunit of the Spt-Ada-Gcn5-acetyltransferase (SAGA) transcriptional cofactor complex. Challenging the dogma, we report here a nontranscriptional role for USP22 via a direct effect on the core cell cycle machinery: that is, the deubiquitylation of the G1 cyclin D1 (CCND1). Deubiquitylation by USP22 protects CCND1 from proteasome-mediated degradation and occurs separately from the canonical phosphorylation/ubiquitylation mechanism previously shown to regulate CCND1 stability. We demonstrate that control of CCND1 is a key mechanism by which USP22 mediates its known role in cell cycle progression. Finally, USP22 and CCND1 levels correlate in patient lung and colorectal cancer samples and our preclinical studies indicate that targeting USP22 in combination with CDK inhibitors may offer an approach for treating cancer patients whose tumors exhibit elevated CCND1.**

pathway distinct from protein-destabilizing GSK3 $\beta$  phosphorylation and ultimately protects CCND1 from proteasome-mediated degradation (16, 17). D-type cyclins are rate-limiting regulators of G1-S progression in mammalian cells, primarily via their ability to bind and activate the kinases CDK4 and CDK6 (18). Consistent with the control of CCND1 levels by USP22, Food and Drug Administration (FDA)-approved CDK inhibitors are epistatic with USP22 depletion in the growth suppression of cancer cells. Collectively, these findings define a previously unknown pathway of CCND1 regulation and establish a mechanistic link between USP22, CCND1, and cancer cell cycle progression that expands potential therapeutic strategies for cancers with elevated CCND1.

## Results

**Loss of USP22 in Cancer Cells Results in Defective G1/S Cell Cycle Transition.** The ubiquitin hydrolase USP22 has been causally linked to aggressive growth in human tumor cells in vitro and in vivo (1, 8–13, 19–25). Consistent with this, depletion of USP22 in the nonsmall-cell lung cancer line H1299 results in a marked decrease in cell number (Fig. 1 A and B). This observation was

USP22 | CCND1 | cell cycle | SAGA | deubiquitylation

Ubiquitin-specific peptidase 22 (USP22) is a deubiquitylating enzyme that functions as a subunit of the human Spt-Ada-Gcn5-acetyltransferase (SAGA) transcriptional coactivator complex (1–3). Within SAGA, USP22 catalyzes histone H2A and H2B deubiquitylation, thereby altering chromatin structure and gene transcription (1, 2, 4). Elevated USP22 expression is tightly correlated with aggressive behavior in human cancer and it was initially identified as a member of an 11-gene “death-from-cancer” signature linked to poor prognosis (5, 6). Further investigation found that USP22 is not only a marker of aggressive tumor phenotypes but also plays a causal role in driving aggressive cancer. At the cellular level, USP22 is critical for progression through the G1 phase of the cell cycle (7–13).

Biochemically, USP22 deubiquitylates substrates beyond nucleosomal histones, including FBP1 and TRF1 (14, 15). However, there has been limited success in linking direct substrates of USP22 to its potent biological phenotypes, including its role in appropriate G1-S transition. To generate a comprehensive understanding of USP22 substrates and how they might contribute to USP22 function, we conducted an unbiased proteome-wide screen. While the screen confirmed known substrates of USP22, including histones H2A and H2B, the sole component of the core cell cycle machinery identified as a USP22 substrate in this screen was the G1 phase cyclin CCND1.

Further analysis of the USP22-CCND1 relationship revealed that USP22 directly reverses polyubiquitylation of CCND1 via a

## Significance

The deubiquitylase USP22 is frequently overexpressed in cancer and contributes to tumorigenesis by driving cell cycle progression. Current models define USP22 as functional mediator of gene regulation and chromatin modification, working within the SAGA transcriptional cofactor complex. Here we report a catalytic role for USP22 distinct from its well-characterized transcription regulatory capacity. USP22 directly stabilizes the essential G1-cyclin, CCND1, protecting it from proteasome-mediated degradation via deubiquitylation. Our findings reveal a pathway that regulates CCND1, while also raising the possibility that simultaneously targeting USP22 may allow the use of less toxic doses of the new wave of cancer therapies that target the cyclin/CDK complex. Finally, these results provide a mechanistic explanation for the effects of USP22 in cancer cell cycle control.

Author contributions: V.J.G., T.J.S., J.A.D., and S.B.M. designed research; V.J.G., T.J.S., A.R.P., Y.S., F.W., and S.Q. performed research; K.E.K., H.R., T.B., and J.A.D. contributed new reagents/analytic tools; V.J.G., T.J.S., and S.B.M. analyzed data; and V.J.G. and S.B.M. wrote the paper.

Conflict of interest statement: The authors declare no conflict of interest.

This article is a PNAS Direct Submission.

This open access article is distributed under [Creative Commons Attribution-NonCommercial-NoDerivatives License 4.0 \(CC BY-NC-ND\)](https://creativecommons.org/licenses/by-nc-nd/4.0/).

<sup>1</sup>To whom correspondence should be addressed. Email: [steven.mcmahon@jefferson.edu](mailto:steven.mcmahon@jefferson.edu).

This article contains supporting information online at [www.pnas.org/lookup/suppl/doi:10.1073/pnas.1807704115/-DCSupplemental](http://www.pnas.org/lookup/suppl/doi:10.1073/pnas.1807704115/-DCSupplemental).

Published online September 17, 2018.

consistent using USP22 shRNA vectors efficiently targeting distinct regions of the transcript (Fig. 1C). A priori, the decrease in cell number caused by USP22 depletion might result from either a defect in cell cycle progression or enhanced cell death. However, directly assessing cell viability and apoptosis revealed no significant changes upon USP22 depletion (Fig. 1D–H), suggesting that the defect in cell number was unlikely due strictly to cell death. In contrast, cell cycle analysis revealed that USP22 knockdown elicited a substantial increase in population of cells in the G1 phase and a concomitant reduction of cells in S phase (Fig. 1I and J and *SI Appendix, Fig. S1 F and G*). G1 arrest in the absence of increased cell death was also observed following USP22 depletion in the human breast cancer cell line MCF7, human prostate cancer cell line PC3, and human colon cancer cell line HCT116 (*SI Appendix, Figs. S1–S3*).

**Proteomic Analysis (UbiScan) Identifies CCND1 as a Candidate Substrate of USP22.** To understand the mechanistic basis of this cell cycle phenotype, a proteome-wide screen for USP22-dependent ubiquitylation was conducted. This screen analyzed the USP22-dependent accumulation of ubiquitylated proteins in HCT116 cells, where protein degradation was blocked by inhibition of the proteasome. This analysis relies on affinity capture of ubiquitylated peptides using an antibody specific for the di-glycine tag that remains linked to ubiquitylated lysine residues following proteolysis by trypsin (26). Enriched ubiquitylated peptides were subject to LC-MS/MS analysis for quantitative profiling of nonredundant ubiquitylated sequences searched against National Center for Biotechnology (NCBI) *Homo*

*sapiens* protein database. Significant hits were defined with a 2.5-fold cut-off between compared samples, a minimum peptide intensity of  $2 \times 10^5$ , and a maximum percent coefficient of variation of 50%. With the stringency parameters outlined above, 145 peptides were identified whose ubiquitylation levels increased upon USP22 depletion. In addition, 203 peptides were identified whose ubiquitylation levels decreased. As a ubiquitin hydrolase, USP22 depletion results in an increase in the ubiquitylation status of its direct substrates. Conversely, proteins containing ubiquitylation sites that decrease upon USP22 depletion are presumably indirect targets.

Relative to the goal of understanding the mechanism by which USP22 impacts cell cycle regulation, proteomic analysis revealed the D-type cyclin CCND1 as a potential USP22 substrate in this screen. Of the 348 high-confidence proteins detected with altered ubiquitylation status in the absence of USP22, CCND1 was the only cyclin, CDK, or CDK inhibitor identified. Upon USP22 depletion, five distinct lysines within CCND1 were detected as potential sites of elevated ubiquitylation (K33, K46, K50, K112, and K114) with an increase relative to control ranging from 2.5- to 3.5-fold (Fig. 2A–C and *SI Appendix, Table S1*). Classifying ubiquitylation patterns relied on the identification of single or multiple di-glycine remnants on specific CCND1 peptides. Dual di-glycine remnants at both K33 and K46 were observed on a single peptide, indicating simultaneous ubiquitylation events on the same CCND1 molecule. As K112 and K114 can reside in the same peptide after partial cleavage by trypsin, this analysis did not provide an unambiguous identification of which lysine is the natural acceptor site.

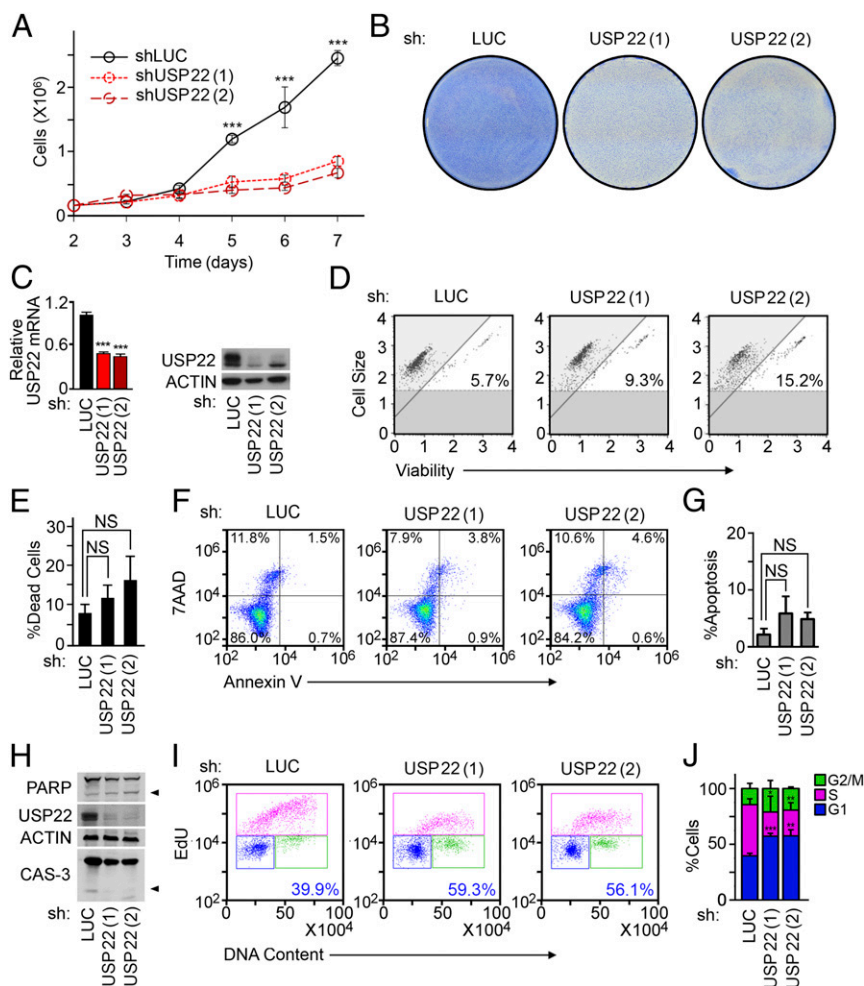


**Fig. 1.** Loss of USP22 in cancer cells results in G1-phase cell cycle arrest. H1299 human lung cancer cells depleted of USP22 via infection with an shRNA-encoding lentivirus (or a luciferase shRNA as a control). After selection, cells counted and plated at 80,000 cells/mL on day 2 postinfection. (A) Cell number determined by direct counting of triplicate wells in a six-well plate via hemocytometer at the indicated time points. (B) Colony growth assessed via fixation and methylene blue staining of foci at day 7 postinfection. (C) Efficient knockdown of USP22 confirmed by both qRT-PCR and immunoblot (IB). (D) Cell viability quantified via flow cytometry. (E) Quantification of three experimental replicates representing average and SD of percent cell death, based on permeability. (F) Apoptosis measured by Annexin V-PE and 7AAD DNA staining, quantified by flow cytometry. (G) Quantification of three experimental replicates representing average and SD of percent apoptosis based on population of Annexin V-PE<sup>+</sup> cells. NS, not significant. (H) PARP and CASPASE-3 (CAS-3) cleavage demonstrated by IB. The black arrowhead indicates cleaved species. (I) Progression through the cell cycle determined by EdU incorporation and PI staining followed by flow cytometry; the percent of cells in G1 phase is represented in blue. (J) Quantification of three experimental replicates of cell cycle phase distribution. Error bars indicate SD based on three independent experiments. \**P* < 0.05, \*\**P* < 0.02, \*\*\**P* < 0.005.

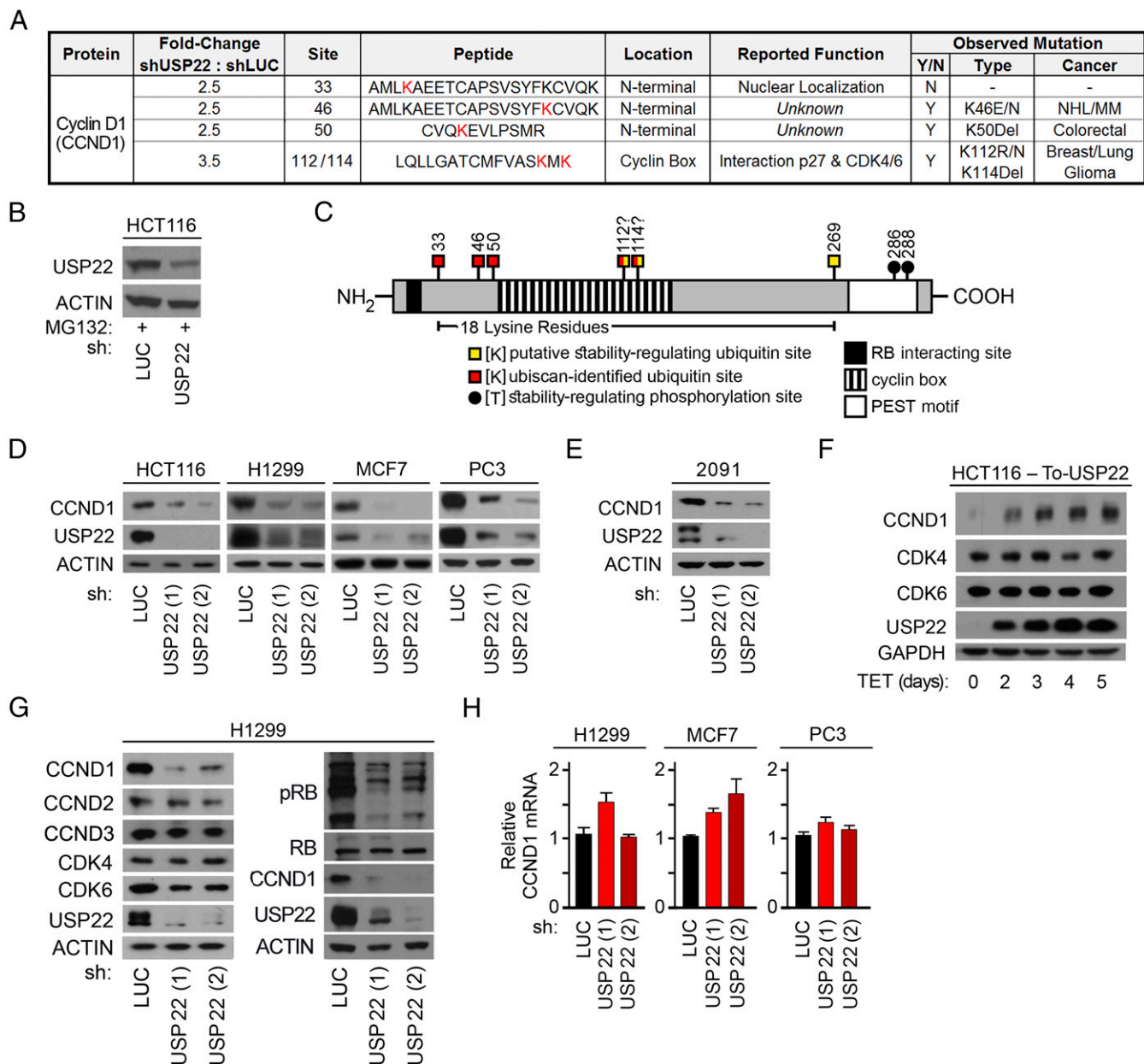


**Fig. 2.** Proteomic analysis (UbiScan) identifies CCND1 as a candidate substrate of USP22. (A) USP22-dependent regulation of CCND1 ubiquitylation status identified by UbiScan. This unbiased proteomic analysis was performed in HCT116 cells following USP22 depletion and proteasome inhibition. Ubiquitylated lysine residues and their reported functional roles in CCND1 are listed, along with potential links to cancer mutations. (B) Efficient knockdown of USP22 shown by IB for samples subjected to UbiScan analysis. (C) Schematic representation of CCND1 indicating known posttranslational modifications and ubiquitylated residues identified by UbiScan. (D) Levels of CCND1 protein following USP22 depletion determined by IB in HCT116, H1299, MCF7, and PC3 cells. (E) CCND1 protein levels following loss of USP22 evaluated in nonmalignant, human fibroblast 2091 cells. (F) FLAG-tagged USP22 was ectopically expressed in HCT116 cells via a stably integrated tetracycline-inducible vector. CCND1 and CDK4/6 protein levels assessed following USP22 induction for the indicated time points. (G) Protein levels of phosphorylated pRB, RB, CCND1, CCND2, CCND3, CDK4, and CDK6 assessed by IB in H1299 cells. (H) CCND1 mRNA levels measured by qRT-PCR following USP22 depletion in H1299, MCF7, and PC3 cells.

The functional relevance of USP22 regulated ubiquitylation was assessed by examining steady-state CCND1 levels upon USP22 depletion. In the colon cancer cell line HCT116 used in the original screen and in the cancer lines H1299, MCF7, and PC3 (Fig. 2D), USP22 depletion resulted in a decrease in CCND1 protein levels. This effect on steady-state CCND1 was also observed in the human dermal fibroblast cell line 2091, linking USP22 to the regulation of CCND1 in both normal and malignant cells (Fig. 2E). Furthermore, USP22 regulation of CCND1 occurred independently of p53 activity (*SI Appendix,*

Fig. S4E). The elevated ubiquitylation and decreased steady-state levels of CCND1 seen after USP22 depletion suggest that deubiquitylation of CCND1 by USP22 may protect it from proteasomal degradation.

Levels of both USP22 and CCND1 are elevated in human cancer, raising the possibility that elevated USP22 might protect CCND1 from degradation. To assess this, a conditional allele of USP22 was ectopically expressed. Over a 5-d course of USP22 induction, CCND1 levels increased (Fig. 2F). Levels of the CCND1 partners CDK4 and CDK6 were simultaneously

examined, with no apparent impact of USP22 induction on levels of either kinase.

D-type cyclins are the rate-limiting partners of CDK4/6, which together form an active kinase complex whose canonical substrates include the retinoblastoma (RB) tumor suppressor protein (27, 28). Phosphorylation of RB by CCND-CDK4/6 is essential for efficient progression through the G1 to S transition of the cell cycle (29–31). To probe the functional consequences of USP22-mediated regulation of CCND1 protein levels, the phosphorylation status of RB was assessed. Depletion of USP22 from H1299 cells resulted in the expected decrease in CCND1 levels and this was accompanied by a defect in RB phosphorylation (Fig. 2G). Consistent with results from conditional USP22 expression, depletion of USP22 had no substantive impact on CDK4 or CDK6 protein levels. Similarly, levels of the CCND1 family members CCND2 and CCND3 were not impacted by USP22 depletion, suggesting separate regulatory mechanisms for these otherwise closely related proteins (Fig. 2G and *SI Appendix, Fig. S5*). USP22 is a critical component of the SAGA transcription regulatory complex, and therefore might exert its impact on CCND1 protein levels indirectly via changes in transcription of the *CCND1* locus. However, quantitative analysis of CCND1 transcript levels in cells revealed no decrease after USP22 depletion, suggesting that USP22 affects CCND1 protein stability (Fig. 2H). In addition to USP22, the SAGA complex contains ~20 proteins, including the GCN5/KAT2A acetyltransferase and ATXN7L3, a subunit tightly bound to USP22 and critical for its catalytic activity (32). Depletion of either of these SAGA subunits resulted in decreased CCND1 protein, which phenocopied the decrease in CCND1 observed upon USP22 depletion. As with USP22, the effects of GCN5 and ATXN7L3 on CCND1 protein could not be explained by an effect on CCND1 mRNA (*SI Appendix, Fig. S6*).

**USP22 Stabilizes CCND1 Protein, Protecting It from Proteasome-Mediated Degradation.** Collectively, these findings suggest a model in which USP22 directly deubiquitylates CCND1, thereby

protecting it from polyubiquitylation and proteasome-mediated degradation. To test this model, the ability of proteasome inhibition to reverse the effects of USP22 depletion on CCND1 protein levels was tested. In cells depleted of USP22, treatment with either of two proteasome inhibitors (MG132 or epoxomicin) largely rescued the loss of CCND1 protein (Fig. 3A). This proteasome-dependent control of CCND1 by USP22 was consistent in human cell lines from multiple lineages, using multiple shRNAs (Fig. 3B). In comparison, treatment with a pan calpain inhibitor (ALLN) resulted in only a modest rescue of CCND1 levels (Fig. 3A). Taken together, these data suggest that USP22 regulates CCND1 via a proteasome-dependent mechanism.

Providing further evidence that USP22 controls CCND1 levels largely via effects on the CCND1 protein, ectopically expressed CCND1 was sensitive to USP22 depletion to an extent similar to endogenously expressed CCND1. Furthermore, similar to endogenous CCND1, the impact of USP22 depletion on ectopic CCND1 was largely rescued by proteasome inhibition (Fig. 3C).

Protection of CCND1 from polyubiquitylation and degradation by USP22 predicts an impact on CCND1 protein half-life. This was assessed using cycloheximide (CHX) to block CCND1 translation and subsequently following the protein decay rate over time. In control cells, this analysis demonstrated a relatively short half-life for CCND1 (~20 min), consistent with previous reports (33). Depletion of USP22 resulted in an even more rapid destruction of CCND1, yielding a half-life of ~10 min. This acceleration in CCND1 decay rate results from enhanced proteasome-mediated degradation, as treatment with epoxomicin (EPX) fully stabilized the protein (Fig. 3D–F).

**USP22 Catalyzes CCND1 Protein Polyubiquitylation Independent of T286 Phosphorylation.** An additional prediction of the model is that USP22 depletion should result in the accumulation of high molecular-weight species of polyubiquitylated CCND1, particularly in the context of proteasome inhibition. Long exposure of a Western blot for CCND1 from USP22-depleted cells indeed

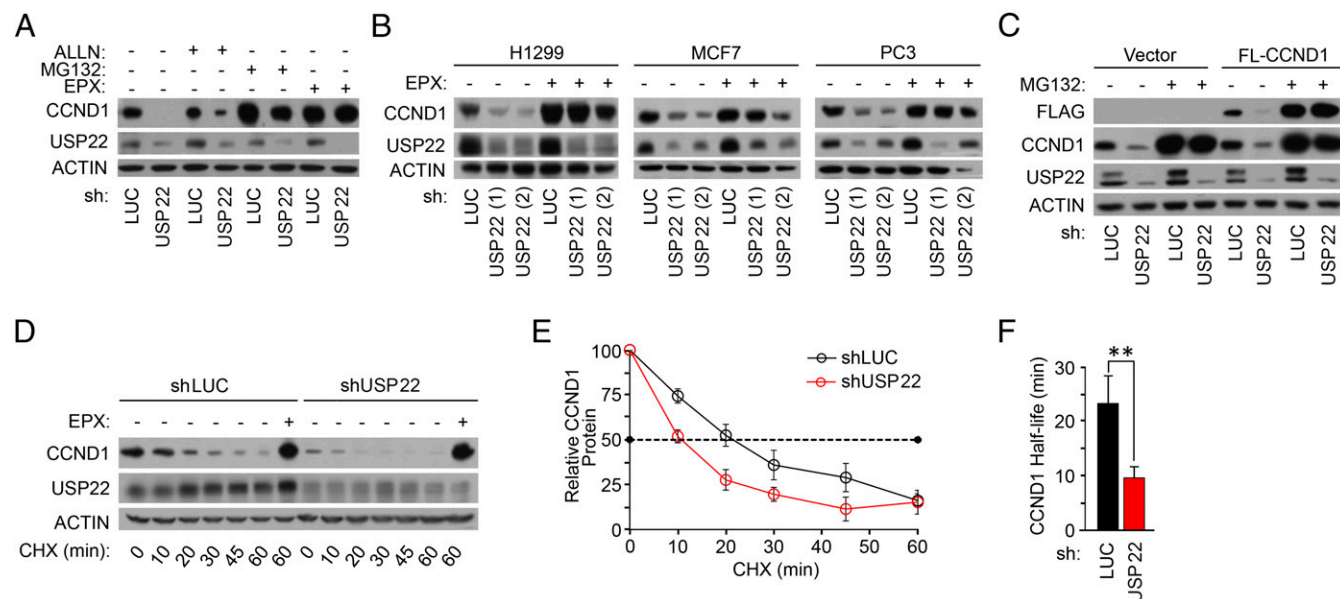


**Fig. 3.** USP22 protects CCND1 protein from proteasome-mediated degradation. (A) CCND1 protein levels assessed in the presence of the proteasome inhibitors MG132 or EPX or the Calpain I inhibitor ALLN in H1299 cells. (B) USP22 depletion in H1299, MCF7, and PC3 cells accomplished using two distinct shRNA constructs. CCND1 protein levels assessed in the presence or absence of the proteasome inhibitor EPX. (C) The effect of USP22 depletion on the levels of ectopically expressed CCND1 assessed in H1299 cells. The impact of proteasome inhibition examined following MG132 treatment. (D) CCND1 protein half-life evaluated by treatment of cells with CHX for the indicated times. (E) CCND1 protein levels quantified for three CHX time-course experiments, followed by normalization to actin. Initial CCND1 levels set to 100%. (F) Bar graph representing the average and SD of CCND1 protein half-life for the experiments plotted in E. Error bars indicate SD based on three independent experiments. \*\* $P < 0.02$ .

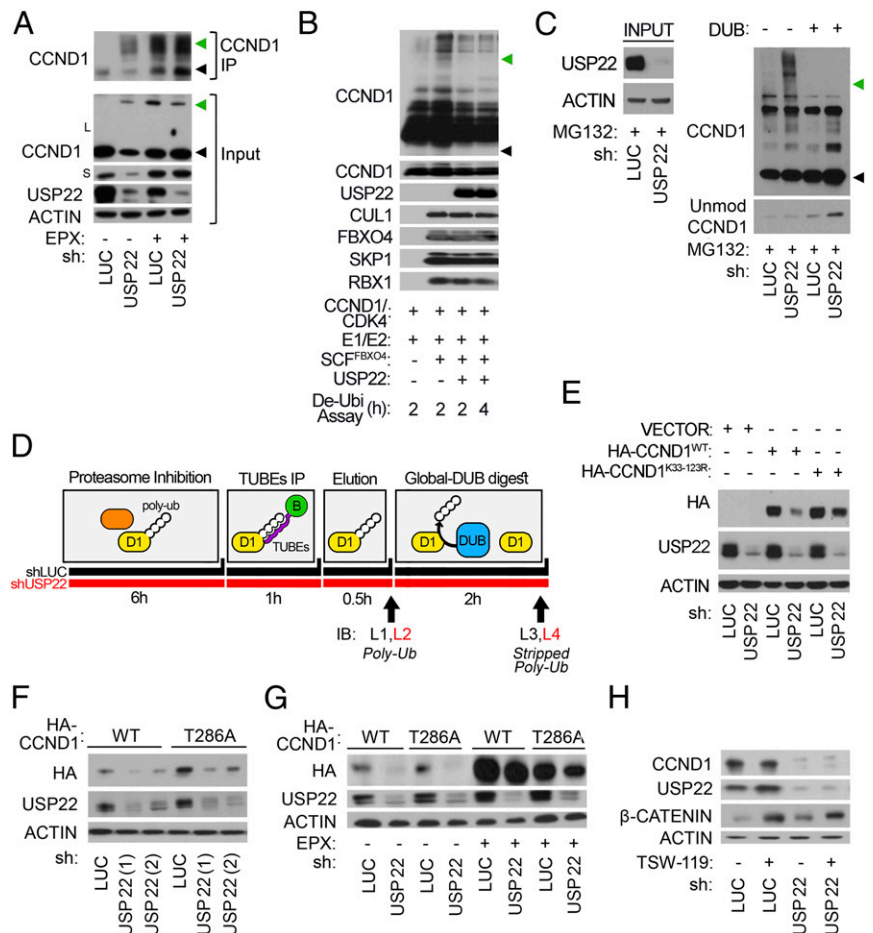
revealed high molecular-weight species of CCND1. These species appear to represent polyubiquitylated CCND1 as proteasome inhibition triggered their appearance, even in the absence of USP22 depletion (Fig. 4A and *SI Appendix*, Fig. S7A). Transient interactions between a deubiquitylating enzyme and its substrate are often difficult to capture, presumably due to the rapid hydrolysis of the isopeptide bond linking ubiquitin to a target lysine residue (34). However, ectopic expression of both proteins followed by immunoprecipitation (IP) demonstrated an *in vivo* interaction (*SI Appendix*, Fig. S7B). To address whether CCND1 is a direct substrate of USP22, these proteins were subjected to an *in vitro* ubiquitylation and successive deubiquitylation reaction, using a strategy described previously (35). The SCF<sup>FBXO4</sup>, CCND1/CDK4, and USP22 complexes were purified from Sf9 cells infected with the relevant baculovirus expression vectors. To ubiquitylate CCND1 protein, the SCF<sup>FBXO4</sup> complex and CCND1/CDK4 complex were combined with E1, E2 (UbcH5a), ATP, and ubiquitin. Following ubiquitylation, samples were incubated with or without purified USP22 complex for times indicated. The addition of purified USP22 complex to the reaction resulted in a marked decrease in polyubiquitylated CCND1 (Fig. 4B). Alternative *in vitro* assays performed with complexes preserved and isolated from mammalian cells further demonstrated deubiquitylation of CCND1 by USP22 (*SI Appendix*, Fig. S7C).

To define whether the high molecular-weight species of CCND1 that appear upon USP22 depletion represent polyubiquitylated molecules, lysates were subjected to purification using tandem ubiquitin binding elements (TUBEs). Subjecting lysates from USP22-depleted cells to this *in vitro* purification demonstrated that the high molecular-weight forms of CCND1 reflected polyubiquitylated species. Addition of a promiscuous global ubiquitin hydrolase to the reaction collapsed the high molecular-weight species of CCND1 to the molecular weight of unmodified CCND1, confirming their identity as polyubiquitin-bearing molecules (Fig. 4C and D).

Previous work suggested that mutation of all CCND1 lysines to arginine confers protection from proteasome-dependent degradation, while single mutations only offered a modest increase in the stability of CCND1 (36). To determine whether regulation of CCND1 by USP22 depends on the presence of lysine residues, an HA-tagged CCND1 mutant containing arginine conversions of all lysine residues from K33 to K123, was assessed for sensitivity to USP22. Compared with HA-CCND1 WT, HA-CCND1 K33-123R partially rescued the destabilization of CCND1 observed with loss of USP22 (Fig. 4E). Collectively, these data imply that USP22 can directly remove polyubiquitin chains from CCND1 lysine residues and protect it from proteasome-mediated degradation.

Previously, the ubiquitin hydrolase USP2 was reported to deubiquitylate CCND1 (37). In H1299 cells, depletion of either

**Fig. 4.** USP22 directly deubiquitylates CCND1 protein independent of phosphorylation at T286. (A) H1299 cell lysates subjected to an endogenous CCND1 IP under nonreducing conditions using A/G beads. Precipitates probed for CCND1 to detect high molecular-weight species, presumably ubiquitylated CCND1. (B) Sf9 cells were infected with baculovirus-expressing Flag-Fbxo4, Flag-cyclin D1, CDK4, HA- $\alpha$ -B-crystallin, HA-Cul1, HA-Skp1, and HA-Rbx1. SCF<sup>Fbxo4</sup> complex and CCND1/CDK4 complex then purified using anti-FLAG M2 and combined with E1/E2 ligases, ATP, and ubiquitin for 30 min at 37 °C to ubiquitylate CCND1 protein. Postubiquitylation assay, the CCND1/CDK4 complex was isolated and incubated with or without USP22 at 37 °C for indicated times in deubiquitylation buffer. Protein levels detected by IB; high molecular-weight CCND1 species indicative of polyubiquitylated CCND1. (C) HCT116 cell lysates subjected to *in vitro* analysis of CCND1 ubiquitylation status following USP22 depletion using UbiTest, as described in the *Materials and Methods*. Cells treated with MG132 before harvest and lysates generated using buffer containing protease mixture inhibitor, pan DUB inhibitor PR619, and the conventional chelator o-phenanthroline. Eluates then either left undigested (lanes 1 and 2) or subsequently digested with a global-DUB to strip polyubiquitin (lanes 3 and 4). Protein levels were detected by IB. The black arrowheads indicate unit length CCND1 (nonubiquitylated) and the green arrowheads indicate high molecular-weight species presumably representing ubiquitylated CCND1. (D) Schematic representing UbiTest experimental design from C. (E) H1299 cells made to express HA-tagged CCND1 WT or mutant with lysines from K33-K123. USP22 depleted in cells with shRNA-mediated lentivirus and CCND1 protein levels were assessed via anti-HA by IB. (F) HA-tagged CCND1 was expressed in H1299 cells as either WT or with phosphorylation site mutation T286A. Following USP22 depletion with two distinct shRNA constructs, cells were lysed and CCND1 protein levels were assessed by IB. (G) H1299 cells expressing the WT or T286A isoforms of HA-tagged CCND1 were subjected to USP22 depletion and subsequent analysis by IB in the presence or absence of proteasome inhibition (EPX). (H) Phosphorylation-dependence of USP22-depletion induced CCND1 degradation was assessed by inhibition of the T286 kinase GSK3 $\beta$  via treatment with TSW-119. Following depletion of USP22, CCND1 protein levels were assessed by IB. The established GSK3 $\beta$  pathway substrate  $\beta$ -catenin was included as control for TSW119 efficacy.



USP2 or USP22 resulted in similar decreases in steady-state CCND1, and effects of both deubiquitinating enzymes (DUBs) were partially rescued by proteasome inhibition (*SI Appendix, Fig. S8A*). No interdependent changes in protein levels were detected in USP2 and USP22 upon knockdown, suggesting that USP22 depletion does not result in decreased steady-state CCND1 via an indirect effect on USP2 levels. Moreover, loss of CCND1 upon depletion of either USP2 or USP22 had similar functional consequences and similarly increased high molecular-weight polyubiquitinated CCND1 species (*SI Appendix, Fig. S8 B and C*).

The best-characterized pathway of CCND1 degradation relies on its phosphorylation-dependent export from the nucleus followed by polyubiquitylation and proteasome-mediated degradation in the cytoplasm (17, 38). To directly test the phosphorylation dependence of the effect of USP22 on CCND1, CCND1 mutants containing alanine conversions at either T286 or T288 were assessed for sensitivity to USP22. For both of these phosphorylation-defective mutants, depletion of USP22 had effects similar to its effect on WT CCND1 (Fig. 4*F* and *SI Appendix, Fig. S9A*). Further analysis demonstrated that inhibition of proteolysis rescued the USP22 effect on mutant T286A CCND1, as it did for WT CCND1 (Fig. 4*G*). Previous studies have identified GSK3 $\beta$  as a primary kinase responsible for CCND1 phosphorylation at T286 (39). To confirm that USP22 affects endogenous CCND1 stability independent of phosphorylation at this site, USP22-depleted cells were treated with the GSK3 $\beta$  inhibitor TSW-119. Consistent with the observation that USP22 depletion affects mutant T286A CCND1 stability, inhibiting phosphorylation at T286 with TSW-119 resulted in no alteration of endogenous CCND1 protein or phosphorylated CCND1 (Fig. 4*H* and *SI Appendix, Fig. S9B*). Because phosphorylation at T286 acts as a precursor to nuclear export, CCND1 levels in separate cellular fractions were assessed upon depletion of known CCND1-dependent USP2 and USP22. CCND1 in whole-cell lysates and in the cytoplasmic fraction were both decreased upon depletion of USP22 or USP2. A long exposure of the Western blots suggests that the nuclear pool of CCND1 decreased following USP22 depletion, while USP2 depletion had little effect (*SI Appendix, Fig. S10A*). To gain a more precise understanding of the cellular CCND1 pools that are targeted by USP22, nuclear fractions were further subdivided into chromatin-bound and chromatin-free protein pools (*SI Appendix, Fig. S10B*). These findings suggest that USP22 and USP2 may have distinct mechanisms of action on CCND1, with USP22 controlling a CCND1 degradation pathway that is at least partially distinct from the canonical, phosphorylation-dependent pathway.

**Ectopic CCND1 Protein Partially Rescues the Aberrant Cell Proliferation Phenotype Observed with USP22 Depletion.** As reported here and elsewhere, USP22 plays a significant role in cell cycle progression, with the greatest impact on the G1 phase (Fig. 1). Because CCND1 is among the central regulators of G1 progression in mammalian cells, we tested the hypothesis that CCND1 deficiency contributes to the effect of USP22 depletion on G1 progression. Despite data shown in Fig. 3 demonstrating USP22 regulating exogenous CCND1, a modest level of CCND1 was established by transient expression (Fig. 5*A*). Ectopic expression of CCND1 in cells depleted of USP22 caused an increase in proliferation relative to control cells (Fig. 5*B* and *C*). Further analysis confirmed that this rescue occurred primarily via a reduction in transit through G1 (Fig. 5*D*). That the aberrant cell proliferation observed with USP22 depletion can be partially rescued by ectopic CCND1 protein suggests that stabilization of CCND1 is a key event in the USP22-mediated regulation of the cell cycle.

**USP22 Regulation of CCND1 Has Clinical Consequences as CDK4/6 Treatment Rescues the G1 Phenotype Associated with USP22 Overexpression.** Overexpression of CCND1 is a well-established hallmark of human cancer (40, 41). Similarly, USP22 overexpression is conserved among many aggressive forms of cancer (5, 6, 42). To assess any potential correlation between USP22 elevation and CCND1 elevation, human tumor tissue microarrays were quantified for levels of each protein. Among 110 colorectal carcinoma samples and 110 lung carcinoma samples (Fig. 6*A* and *B* and *SI Appendix, Fig. S11*), a significant correlation between CCND1 and USP22 protein levels was observed. Elevated CCND1 activity and expression in cancer can be targeted clinically using FDA-approved CDK inhibitors. The findings presented here suggest that tight regulation of USP22 is essential for G1-S transition via CCND1 regulation, raising the possibility that USP22 might represent a therapeutic target. To assess the therapeutic potential of this pathway, HCT116 cells engineered to overexpress USP22 were treated with the CDK inhibitor PD-0332991. As expected, induction of ectopic USP22 resulted in an enhanced G1 exit (Fig. 6*C* and *D*) and increased CCND1 protein levels (Fig. 6*E*). Strikingly, inhibiting downstream CCND1/CDK activity with PD-0332991 in USP22-overexpressing cells was sufficient to reverse the effect of USP22 on cell-cycle progression. Furthermore, HCT116 cells treated with PD-0332991 demonstrated a similar defect in G1-S transition to that of cells with reduced USP22 expression. Concomitant depletion of USP22 and inhibition of CDK4/6 resulted in no additive cell cycle or death response (*SI*

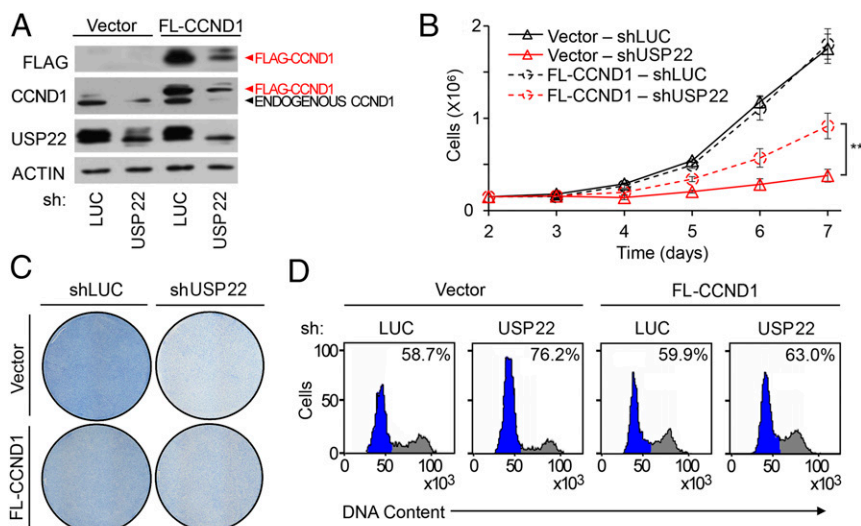


**Fig. 5.** Ectopic expression of CCND1 provides a partial genetic rescue of the cell cycle phenotype observed with USP22 depletion. H1299 cells were transfected with a vector encoding 3XFLAG-tagged CCND1, followed by USP22 depletion. (A) Immunoblot demonstrating efficient knockdown of USP22, exogenous 3XFLAG-CCND1, and endogenous CCND1 expression. (B) Cell number was determined by manual counting of experimental triplicates at each of the postdepletion time points indicated. Error bars indicate SD based on three independent experiments. (C) Methylene blue-stained foci of representative plates from B. (D) At day 7 following USP22 depletion, cells were harvested and cell cycle profile was determined by PI staining and flow cytometry. G1-phase cells were gated (in blue) as percent of the total population. \*\* $P < 0.02$ .

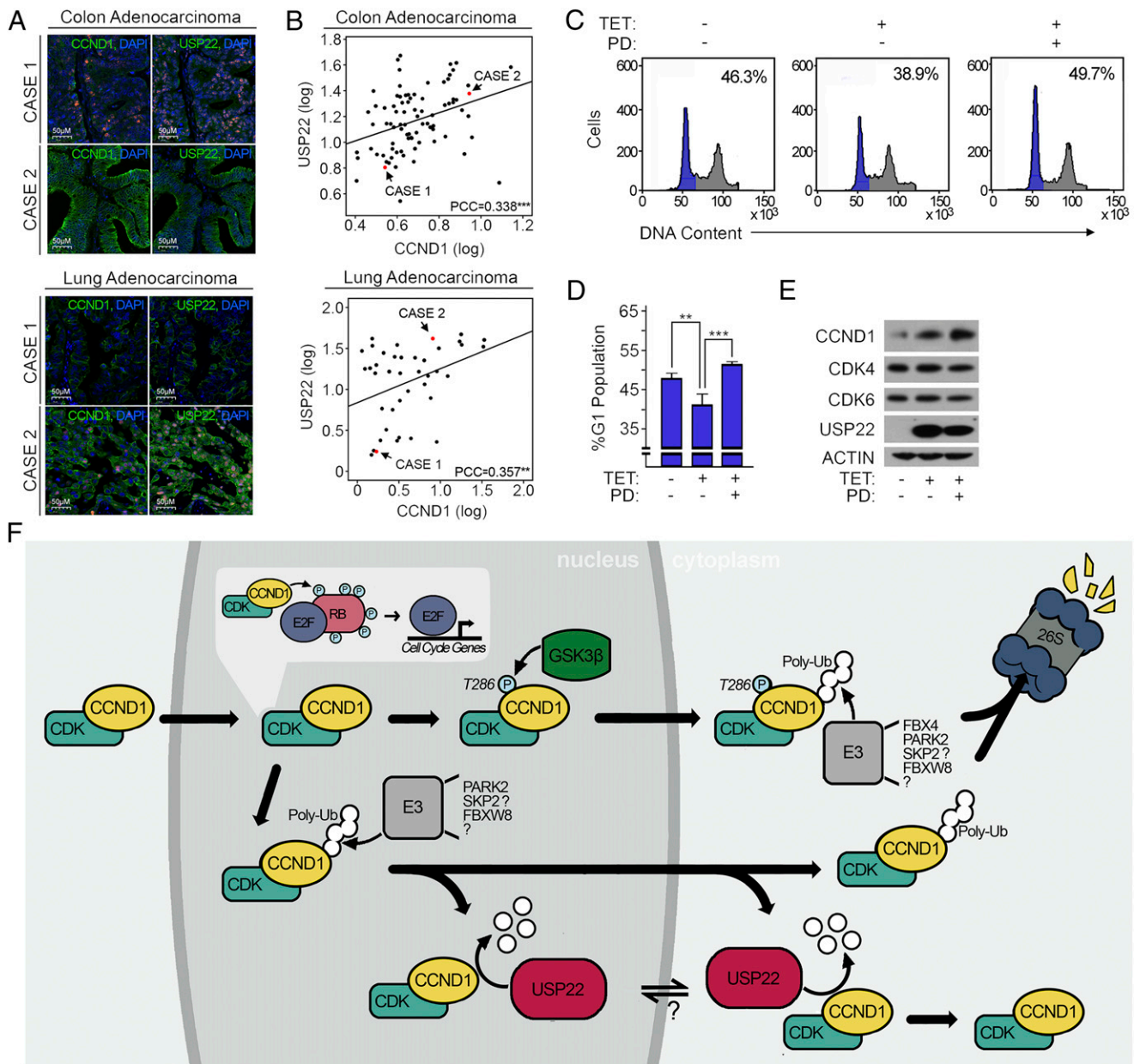


**Fig. 6.** CCND1 and USP22 protein levels correlate in patient samples from lung and colon adenocarcinoma and CDK4/6i treatment rescues the G1 phenotype associated with USP22 overexpression. (A) Representative images of serial sections of colon adenocarcinoma or lung adenocarcinoma BioMax tissue microarrays stained with DAPI and either USP22 or CCND1 antibodies. (B) Graphical representation of USP22(log) expression against CCND1(log) expression in each of the 120 cases with representative cases is indicated on the graph. [Pearson's correlation coefficient (PCC) of 0.338 for colon adenocarcinoma or 0.357 for lung adenocarcinoma.] (C) FLAG-tagged USP22 was ectopically expressed in HCT116 cells via a stably integrated tetracycline-inducible vector. Following USP22 induction and treatment with selective CDK4/6 inhibitor PD-0332991 (PD), cells were harvested and cell cycle profile was determined by assessment of DNA content with PI staining and flow cytometry. G1-phase cells were gated (in blue) as percent of the total population. (D) Quantification of cell cycle phase distribution. Error bars indicate SD based on three independent experiments. (E) Induction of ectopic USP22 and increased CCND1 protein levels were assessed by IB.  $^{**}P < 0.02$ ,  $^{***}P < 0.005$ . (F) A schematic representing the proposed model of CCND1 stabilization by deubiquitylase USP22. CCND1-CDK4/6 complex advances cell cycling via hyperphosphorylating RB, which in turn releases E2F transcription factor from an inhibitory constraint and enables the expression of genes required for G1-S phase transition. To regulate rapid turnover, CCND1-CDK4/6 can incur phosphorylation at Thr286 by GSK3 $\beta$ , a precursor to nuclear export and subsequent polyubiquitylation by distinct E3 ligases (e.g., FBX4, PARK2, SKP2, FBXW8. . .) (66–71). Polyubiquitylated CCND1-CDK4/6 is then targeted for proteasomal degradation. USP22 promotes CCND1 stabilization via removing CCND1 ubiquitin within the nucleus and/or cytoplasm and blocking degradation by the proteasome.

Appendix, Fig. S12), suggesting that USP22 and CDK4/6 may regulate the same pathway in an epistatic manner. Collectively, these findings implicate the DUB USP22 as a key regulator of CCND1, and thereby a potential complement to current therapeutic strategies targeting CCND1/CDK4/6 in cancer. For example, the often severe side effects experienced by patients receiving CDK4/6, might be reduced by use of lower doses in combination with USP22 inhibition.

### Discussion

The role of USP22 in transcription is presumed to result in large part from its ability to remove ubiquitin from nucleosomal histones H2A and H2B (1–3). Empirical studies have demonstrated that USP22 can deubiquitylate nonhistone substrates as well (e.g., TRF1 and FBP) (14, 15). USP22 plays a critical role in progression through the G1-S phase transition of the cell cycle and its activity is

both elevated and required for the aggressive growth of numerous cancer lineages (7–13). [Somewhat paradoxically, a role for USP22 in M phase has been proposed based on evidence that CCNB1 is deubiquitylated by USP22 (43)]. Nonetheless, no known substrate of USP22 explains its central biological phenotype, progression through the G1–S cell cycle transition. These studies were undertaken with the expectation that elucidating the role of USP22 in orchestrating the G1–S progression might advance our understanding of aggressive growth phenotypes in cancer and inform the development of novel therapeutics.

What remains lacking is a mechanistic understanding of which substrates of USP22 mediate these potent effects on proliferation. Here, a proteome-wide analysis in human cells identified proteins whose ubiquitylation is regulated by USP22. This screen identified several high-confidence hits within proteins not previously described as USP22 substrates. As reported above, the G1 cyclin CCND1 was validated experimentally as a direct USP22 substrate. USP22 hydrolyzes ubiquitin at a set of specific lysine residues on CCND1 (K33, K46, 50, K112/114). Functionally, K33 ubiquitylation is implicated in nuclear localization of CCND1 (44), and K112 and K114 ubiquitylation are linked to the interaction of CCND1 with partners, including CDK4/6 (45–47). The ubiquitylation of CCND1 at K46 and K50 has not been previously reported. Notably, several of these ubiquitylation sites are mutated in cancer, with missense mutations at K46 and K112 reported in lymphoma and breast cancer, respectively (36). While the detection of these lysine residues indicates preferred sites affected by USP22, ubiquitylation demonstrates notable promiscuity at the level of individual lysine acceptor sites (48). Previous attempts to uncover specific residues that regulate CCND1 proteasomal degradation have demonstrated single and double lysine residue mutations have only modest effects on CCND1 stability (36). This capacity of USP22 to remove polyubiquitin chains protects CCND1 from proteasomal degradation, thereby doubling its half-life and significantly elevating steady-state CCND1 protein levels. Four central observations highlight the biological relevance of CCND1 as a substrate of USP22. First, the G1-phase cell cycle arrest observed upon depletion of USP22 from human cells is genetically rescued by ectopic expression of CCND1. Second, mimicking the scenario in cancer by modest overexpression of USP22 in cells results in a concomitant increase in steady-state CCND1 protein levels. Third, USP22 protein levels directly correlate with CCND1 levels in tumor tissue samples from both colon and lung cancer patients. Finally, experimentally elevating USP22 levels both increases CCND1 and drives more rapid transit through the G1 phase of the cell cycle, an effect blocked by treatment with the FDA-approved CDK4/6 inhibitor PD-0332991. These findings appear not to be linked to the known effect of USP22 on the SIRT1/p53 pathway (49), because they were observed in both p53-proficient and -deficient cell lines. Collectively these findings support a model in which elevated expression of USP22 contributes to the aggressive growth of cancer cells in part via its ability to deubiquitylate and stabilize the rate-limiting cyclin CCND1, thereby promoting the G1–S transition.

The identification of the USP22–CCND1 enzyme–substrate relationship may explain the previously reported phosphorylation-independent ubiquitylation and degradation of CCND1 (50). Our findings demonstrate that USP22 deubiquitylates CCND1 regardless of phosphorylation events at T286 or T288. Genetic evidence that USP2 and USP22 control distinct CCND1 degradation pathways comes from the observation that these enzymes are not redundant, with depletion of either one sufficient to destabilize CCND1. Independent of CDK interaction, CCND1 binds nuclear receptors (ER $\alpha$ , THR, PPAR $\gamma$ , and AR) to regulate cell proliferation, growth, and differentiation (51). Furthermore, CCND1 regulates transcriptional activation by binding histone acetylases, deacetylases, and coactivators (52). Levels of CCND1 in the cytoplasm decreased following depletion of either USP22 or USP2;

however, both the chromatin-bound and chromatin-free pools of CCND1 were sensitive to USP22 depletion, while USP2 depletion had little effect on either pool. These findings suggest that USP22 and USP2 may regulate CCND1 via distinct pathways/mechanisms.

A number of the observations reported here suggest that USP22 may target the unbound form of CCND1 rather than the CDK-bound form. For example, the K112 and K114 sites on CCND1 identified as USP22 targets reside within the CDK interaction domain. Furthermore, the phosphorylation-independent nature of CCND1 targeting by USP22 may allow new therapeutic strategies for targeting this pathway. For example, the clinical efficacy of CDK4/6 inhibitors in cancer might be complemented by combinatorial treatment with a USP22 inhibitor, thus simultaneously targeting both the CDK-bound and the -free forms of CCND1. More broadly, the identification of the critical cell cycle regulator CCND1 as a substrate of the USP22 subunit of SAGA broadens our understanding of this complex, which has previously been linked primarily to direct effects on transcription.

## Materials and Methods

**Cell Culture, Viral Infection, Transfection, and Treatment.** The human cell lines HCT116, H1299, MCF7, PC3, and 2091 were obtained from American Type Culture Collection (ATCC). The ectopic USP22-inducible HCT116 tetracycline hydrochloride (TET) operable cell line was generated by cloning pcDNA3.1 FLAG-USP22 into the pLenti6.3/V5/TO-DEST vector using the Virapower T-Rex system (ThermoFisher). All cell lines were cultured in DMEM (Mediatech) supplemented with 10% FCS (FBS; Gemini Bio-Products) at 37 °C in 5% CO<sub>2</sub>.

As indicated, cells were infected with lentiviral shRNA plasmids corresponding to USP22 (XM\_042698.6-914s1c1, NM\_015276.1-545s21c1), USP2 (NM\_004205.3-1266s1c1, NM\_004205.3-1554s1c1), ATXN7L3 (NM\_001098833.1-1008s21c1), GCN5 (NM\_021078.1-2484s1c1), and control luciferase shRNA (SHC007) that were obtained from the TRC collection (Sigma-Aldrich). Cells were selected with 8  $\mu$ M puromycin 24 h after infection.

Transfection was performed using Continuum reagents according to the manufacturer's protocol (Gemini Bio-Products). HA-CCND1 WT, HA-CCND1 K33-123R, and HA-CCND1 T286A expression plasmids were kindly provided by E. Dmitrovsky, MD Anderson Cancer Center, Houston, TX. HA-CCND1 T288A mutant was constructed by site-directed mutagenesis using QuikChange (Agilent Technologies). The previously described 3XFLAG-CCND1 WT expression plasmid was kindly provided by R. Pestell, Baruch S. Blumberg Institute, Doylestown, PA (53).

For indicated treatments, MG132 was used at 10  $\mu$ M for 6 h (SelleckChem), EPX at 10  $\mu$ M for 6 h (SelleckChem), ALLN at 100  $\mu$ M for 6 h (Abcam), CHX at 10  $\mu$ g/mL as indicated (Sigma-Aldrich), TET at 2.25  $\mu$ M for 5 d (Sigma-Aldrich), PR619 at 50  $\mu$ M for 30 min (Life Sensors), o-phenanthroline at 5  $\mu$ M for 15 min (Life Sensors), TSW-119 at 1  $\mu$ M for 12 h (Santa Cruz), and PD-0332991 (PD) at 100 nM for 3 d (Sigma-Aldrich).

**Cell Proliferation, Viability, and Cell Cycle.** For growth assays, cells were seeded at equal densities and harvested at the indicated time points. Media and treatments were refreshed every 72 h. Cell number was determined quantitatively by triplicate experiments using Trypan blue exclusion and counting by hemocytometer. Cell density was visualized by methylene blue staining.

Levels of necrotic cells were assessed by Muse Count and Viability Reagent and analyzed using the Muse Cell Analyzer as described by the manufacturer (Millipore). To quantify apoptotic cell death, cells were collected by trypsinization and stained using the Annexin V PE-7AAD apoptosis detection kit (BD Pharmingen). Fluorescence was detected by flow cytometry CytoFlex LX Flow Cytometer (Beckman Coulter).

Cell cycle analysis was conducted using the Click-iT EdU flow cytometry cell proliferation assay where cells were labeled with EdU for 2 h, harvested, and stained according to the manufacturer's instructions (Thermo Fisher). DNA content was measured using propidium iodide (PI) staining for 30 min on cells fixed with 70% ethanol. Cell cycle analysis was processed using the CytoFlex LX.

**Immunoblotting, Cellular Fractionation, Co-IP, and mRNA Analysis.** Cells were harvested and lysed in E1A whole-cell lysate buffer supplemented with protease inhibitor mixture (Sigma-Aldrich) and PR619. Western blotting concentration in lysates was determined using the bicinchoninic acid (BCA) assay and analyzed by SDS/PAGE using antibodies against CCND1 (#2978; Cell Signaling), USP22 (#ab195289; Abcam), USP2 (#8036S; Cell Signaling), CDK4 (#sc-260; Santa Cruz), CDK6 (#3136S; Cell Signaling), FLAG (#F316S; Sigma-Aldrich), HA (#sc-805; Santa Cruz), Ubiquitin (#sc-7905; Santa Cruz), RB (#sc-



50; Santa Cruz), pRB (#sc-271930; Santa Cruz), ATXN7L3 (#A302-800A; Bethyl), GCN5 (#sc-365321; Santa Cruz), CCND2 (#3741T; Cell Signaling), CCND3 (#2936S; Cell Signaling), phospho-CCND1 (#3300T; Cell Signaling), FBXO4 (#YZ1779; YenZym Antibodies), CUL1 (#sc-11384; Santa Cruz), SKP1 (#2156; Cell Signaling), RBX1 (#4397; Cell Signaling), ACTIN (#sc-47778; Santa Cruz),  $\beta$ -CATENIN (#8480; Cell Signaling), GAPDH (#ab9485; Abcam), ORC2 (#559266; Pharmingen), and TUBULIN (#T9026; Sigma-Aldrich).

**Cellular Fractionations Were Performed as Described Previously.** Cellular fractionations were performed as described previously (54). For protein-protein interaction studies, ~750  $\mu$ g of whole-cell lysates was used for IP. FLAG IPs were performed by incubating lysates with 20  $\mu$ L Anti-FLAG M2 Affinity Beads (Sigma-Aldrich) for 16 h at 4 °C before Western blot analysis. Endogenous CCND1 IPs were conducted using 5  $\mu$ g of CCND1 antibody (TA329665; OriGene) for 16 h at 4 °C and precipitates captured using protein A/G beads (Santa Cruz).

Total RNA was extracted using TRIzol (Thermo Fisher) and reverse-transcribed using the High-Capacity cDNA Reverse Transcription Kit (Thermo Fisher) according to the manufacturer's instructions. Real-time PCR was performed using Fast SYBR Green (Thermo Fisher), as described previously (55), using primer sequences are listed in *SI Appendix, Table S1*. In all cases, mRNA levels between samples were normalized to actin levels.

**UbiScan.** Samples were analyzed using the PTMScan method as previously described (56–58). Cellular extracts were prepared in urea lysis buffer, sonicated, centrifuged, reduced with DTT, and alkylated with iodoacetamide. Total protein (15 mg) for each sample was digested with trypsin and purified over C18 columns for enrichment with the Ubiquitin K-GG Remnant Motif antibody (#5562). Enriched peptides were purified over C18 STAGE tips (59). Replicate injections of each sample were run nonsequentially on the instrument. Peptides were eluted using a 72-min linear gradient of acetonitrile in 0.125% formic acid delivered at 280 nL/min. MS/MS spectra were collected in a data-dependent manner with an Orbitrap Elite Hybrid Ion Trap-Orbitrap Mass Spectrometer running XCalibur 2.0.7 SP1 using a top-20 MS/MS method, a dynamic repeat count of one, and a repeat duration of 30 s. Real-time recalibration of mass error was performed using lock mass (60), with a singly charged polysiloxane ion  $m/z = 371.101237$ . MS/MS spectra were evaluated using the Sorcerer platform (61, 62). Files were searched against the NCBI *Homo sapiens* FASTA database. A mass accuracy of  $\pm 50$  ppm was used for precursor ions and 1.0 Da for product ions. Enzyme specificity was limited to trypsin, with at least one tryptic (K- or R-containing) terminus required per peptide and up to four miscleavages allowed. Cysteine carboxamidomethylation was specified as a static modification; oxidation of methionine and a di-glycine remnant on lysine residues were allowed as variable modifications. Reverse decoy databases were included for all searches to estimate false discovery rates, and filtered using a 5% false-discovery rate in Sorcerer. Peptides were also manually filtered using a  $\pm 5$  ppm mass error range and the presence of at least one K-GG on each peptide. All quantitative results were generated using Progenesis v4.1 (Waters Corporation) to extract the integrated peak area of the corresponding peptide assignments. Accuracy of quantitative data was ensured by manual review in Progenesis or in the ion chromatogram files. A 2.5-fold cut-off was used to denote changes between samples and analytical percent coefficient of variation values were calculated for each peptide to determine reproducibility across runs.

**UbiTest.** HCT116 cells were harvested after 6 d of knockdown and 4 h after proteasome inhibition with MG132. Cells were lysed in radioimmunoprecipitation buffer supplemented with protease mixture inhibitor, PR619, and  $\alpha$ -phenanthroline. Protein lysate was incubated with  $\alpha$ -Ub TUBE1 agarose resin, eluted, and digested with global DUB USP2 for 2 h to remove polyubiquitylation, as recommended by the manufacturer (LifeSensors). Undigested and digested samples were analyzed by SDS/PAGE and Western blotting.

**In Vitro Ubiquitylation–Deubiquitylation Assay.** Sf9 cells were infected with baculovirus expressing FLAG-FBXO4, FLAG-CCND1, CDK4, HA- $\alpha$ -B-CRYSTALLIN, HA-CUL1, HA-SKP1, and HA-RBX1. Seventy-two hours postinfection, cells were lysed in Tween 20 buffer [50 mM Hepes (pH 8.0), 150 mM NaCl, 2.5 mM EGTA, 1 mM EDTA, and 0.1% Tween 20 with protease and phosphatase inhibitors]. To generate the DUB module with active USP22, Sf9 cells were infected with baculovirus expressing FLAG-USP22N, ATXN7, ATXN7L3, and HA-ENY2. Forty-eight hours postinfection, cells were lysed in Tween 20 buffer. Cell lysates were subjected to anti-FLAG immunoprecipitation to isolate USP22 within an active DUB complex. The SCF<sup>FBXO4</sup> complex and CCND1/CDK4 complex were purified using anti-FLAG M2 affinity gel.

Beads with SCF<sup>FBXO4</sup> complex and CCND1/CDK4 complex were combined with E1, E2 (UbcH5a), ATP, and ubiquitin for 30 min at 37 °C to achieve ubiquitylated-CCND1 protein. After reaction, beads were washed with deubiquitylation buffer [100 mM Tris (pH 8.0), 1 mM EDTA, 1 mM DTT, and 5% glycerol]. Thereafter, the beads were incubated with or without hDUB USP22 in deubiquitylation buffer for indicated times at 37 °C, as previously described (63). Beads were subsequently boiled in 2 $\times$  loading buffer. Proteins were resolved in 10% SDS/PAGE gel and detected by relative antibodies.

**In Vitro Deubiquitylation Assay.** H1299 cells were transfected with 3XFLAG-CCND1 and HA-Ub, or separately with FLAG-USP22. Cell lysates were subjected to anti-FLAG immunoprecipitation to isolate FLAG-USP22 and 3XFLAG-CCND1 with conjugated HA-Ub. The in vitro enzymatic assay was performed for 2 h at 37 °C, as previously described (63), and subjected to SDS/PAGE analysis.

**Tissue Microarray and Quantitative Immunofluorescence.** Tissue microarrays consisting of formalin-fixed, paraffin-embedded colon or lung cancer specimens were obtained from US Biomax, Inc. The colon array (Cat# BC051110b) consisted of 110 cases of colon adenocarcinoma and 10 normal colon cases. The age range of patients represented on the array was 22–86 y (median 55 y). The lung array (Cat# BC041115d) consisted of 110 cases of mixed-pathology lung cancer and 10 normal lung cases. The age range of patients represented on the array was 15–76 y (median 57 y).

CCND1 and USP22 were detected in clinical colon and lung cancer specimens by immunofluorescence-immunohistochemistry (IF-IHC) performed on Dako Omnis autostainer using the TSA Plus Fluorescence Kit (Perkin-Elmer), as previously described (64). Antigen retrieval was performed using citrate buffer (pH 6.1; Dako). Rabbit monoclonal CCND1 (1:400, M3635; Dako) and rabbit polyclonal USP22 (1:400, HPA044980; Sigma) were individually diluted 1:400 and coincubated with mouse monoclonal antipapillary keratin (clone AE1/AE3, M3515 1:100; Dako) for 45 min. High-resolution digital images of immuno-stained slides were captured using the Panoramic 250 Flash scanner (3DHitech). Quantitative biomarker analysis was performed as previously described (65) using Tissue Studio image analysis software (Definiens). Briefly, user-guided machine learning was used to generate an analysis solution to specifically quantify mean nuclear signal intensity of each biomarker within epithelial DAPI-stained cell nuclei of each tissue core. Statistical analyses were performed in SPSS.

**Statistical Analysis.** Data collected from at least three independent experiments are presented as mean  $\pm$  SD. Statistical testing was performed using SPSS with differences between two groups determined by a Student's *t* test. Significance is denoted in the figures as: \*\*\**P* < 0.005, \*\**P* < 0.02, and \**P* < 0.05.

**ACKNOWLEDGMENTS.** We thank Drs. E. Dmitrovsky (MD Anderson Cancer Center) and R. Pestell (Baruch S. Blumberg Institute) for providing reagents or advice. These studies were supported in part via NIH Grant R01CA182569 (to K.E.K. and S.B.M.). F.W. and T.B. are employed by Progenia Inc., a biotech company engaged in targeting deubiquitylating enzymes for therapeutic benefit. The National Cancer Institute-supported Sloan-Kettering Cancer Center Cancer Genomics facility was used in these studies.

- Zhang XY, et al. (2008) The putative cancer stem cell marker USP22 is a subunit of the human SAGA complex required for activated transcription and cell-cycle progression. *Mol Cell* 29:102–111.
- Zhao Y, et al. (2008) A TFC/STAGA module mediates histone H2A and H2B deubiquitylation, coactivates nuclear receptors, and counteracts heterochromatin silencing. *Mol Cell* 29:92–101.
- Weake VM, et al. (2008) SAGA-mediated H2B deubiquitylation controls the development of neuronal connectivity in the *Drosophila* visual system. *EMBO J* 27:394–405.
- Zhang XY, Pfeiffer HK, Thorne AW, McMahon SB (2008) USP22, an hSAGA subunit and potential cancer stem cell marker, reverses the polycomb-catalyzed ubiquitylation of histone H2A. *Cell Cycle* 7:1522–1524.
- Glinsky GV (2005) Death-from-cancer signatures and stem cell contribution to metastatic cancer. *Cell Cycle* 4:1171–1175.
- Glinsky GV (2007) Stem cell origin of death-from-cancer phenotypes of human prostate and breast cancers. *Stem Cell Rev* 3:79–93.
- Ding F, et al. (2014) USP22 promotes NSCLC tumorigenesis via MDMX up-regulation and subsequent p53 inhibition. *Int J Mol Sci* 16:307–320.
- Ning Z, et al. (2014) USP22 promotes epithelial-mesenchymal transition via the FAK pathway in pancreatic cancer cells. *Oncol Rep* 32:1451–1458.
- Schrengost RS, et al. (2014) USP22 regulates oncogenic signaling pathways to drive lethal cancer progression. *Cancer Res* 74:272–286.
- Hu J, et al. (2015) USP22 promotes tumor progression and induces epithelial-mesenchymal transition in lung adenocarcinoma. *Lung Cancer* 88:239–245.
- Xiao H, et al. (2015) USP22 acts as an oncogene by regulating the stability of cyclooxygenase-2 in non-small cell lung cancer. *Biochem Biophys Res Commun* 460:703–708.
- Li Y, et al. (2017) USP22 drives colorectal cancer invasion and metastasis via epithelial-mesenchymal transition by activating AP4. *Oncotarget* 8:32683–32695.

13. Wang A, et al. (2017) USP22 induces cisplatin resistance in lung adenocarcinoma by regulating  $\gamma$ H2AX-mediated DNA damage repair and Ku70/bax-mediated apoptosis. *Front Pharmacol* 8:274.
14. Atanassov BS, et al. (2009) Gcn5 and SAGA regulate shelterin protein turnover and telomere maintenance. *Mol Cell* 35:352–364.
15. Atanassov BS, Dent SY (2011) USP22 regulates cell proliferation by deubiquitinating the transcriptional regulator FBP1. *EMBO Rep* 12:924–930.
16. Diehl JA, Cheng M, Roussel MF, Sherr CJ (1998) Glycogen synthase kinase-3 $\beta$  regulates cyclin D1 proteolysis and subcellular localization. *Genes Dev* 12:3499–3511.
17. Alt JR, Cleveland JL, Hannink M, Diehl JA (2000) Phosphorylation-dependent regulation of cyclin D1 nuclear export and cyclin D1-dependent cellular transformation. *Genes Dev* 14:3102–3114.
18. Diehl JA (2002) Cycling to cancer with cyclin D1. *Cancer Biol Ther* 1:226–231.
19. Kim D, et al. (2017) Deubiquitinating enzyme USP22 positively regulates c-Myc stability and tumorigenic activity in mammalian and breast cancer cells. *J Cell Physiol* 232:3664–3676.
20. Ling S, et al. (2017) USP22 mediates the multidrug resistance of hepatocellular carcinoma via the SIRT1/AKT/MRP1 signaling pathway. *Mol Oncol* 11:682–695.
21. Ling SB, et al. (2012) Knock-down of USP22 by small interfering RNA interference inhibits HepG2 cell proliferation and induces cell cycle arrest. *Cell Mol Biol* 58:OL1803–OL1808.
22. Liu YL, et al. (2012) USP22 acts as an oncogene by the activation of BMI-1-mediated INK4a/ARF pathway and Akt pathway. *Cell Biochem Biophys* 62:229–235.
23. Liu YL, et al. (2015) The deubiquitinating enzyme activity of USP22 is necessary for regulating HeLa cell growth. *Gene* 572:49–56.
24. Lv L, et al. (2011) Silencing USP22 by asymmetric structure of interfering RNA inhibits proliferation and induces cell cycle arrest in bladder cancer cells. *Mol Cell Biochem* 346:11–21.
25. Ma Y, et al. (2017) USP22 maintains gastric cancer stem cell stemness and promotes gastric cancer progression by stabilizing BMI1 protein. *Oncotarget* 8:33329–33342.
26. Kim W, et al. (2011) Systematic and quantitative assessment of the ubiquitin-modified proteome. *Mol Cell* 44:325–340.
27. Kato J, Matsushime H, Hiebert SW, Ewen ME, Sherr CJ (1993) Direct binding of cyclin D to the retinoblastoma gene product (pRb) and pRb phosphorylation by the cyclin D-dependent kinase CDK4. *Genes Dev* 7:331–342.
28. Ewen ME, et al. (1993) Functional interactions of the retinoblastoma protein with mammalian D-type cyclins. *Cell* 73:487–497.
29. Buchkovich K, Duffy LA, Harlow E (1989) The retinoblastoma protein is phosphorylated during specific phases of the cell cycle. *Cell* 58:1097–1105.
30. Chen PL, Scully P, Shew JY, Wang JY, Lee WH (1989) Phosphorylation of the retinoblastoma gene product is modulated during the cell cycle and cellular differentiation. *Cell* 58:1193–1198.
31. Mihara K, et al. (1989) Cell cycle-dependent regulation of phosphorylation of the human retinoblastoma gene product. *Science* 246:1300–1303.
32. Lang G, et al. (2011) The tightly controlled deubiquitination activity of the human SAGA complex differentially modifies distinct gene regulatory elements. *Mol Cell Biol* 31:3734–3744.
33. Sewing A, et al. (1993) Human cyclin D1 encodes a labile nuclear protein whose synthesis is directly induced by growth factors and suppressed by cyclic AMP. *J Cell Sci* 104:545–555.
34. Hanpude P, Bhattacharya S, Kumar Singh A, Kanti Maiti T (2017) Ubiquitin recognition of BAP1: Understanding its enzymatic function. *Biosci Rep* 37:BSR20171099.
35. Barbash O, Lee EK, Diehl JA (2011) Phosphorylation-dependent regulation of SCF(Fbx4) dimerization and activity involves a novel component, 14-3-3E. *Oncogene* 30:1995–2002.
36. Feng Q, Sekula D, Müller R, Freemantle SJ, Dmitrovsky E (2007) Uncovering residues that regulate cyclin D1 proteasomal degradation. *Oncogene* 26:5098–5106.
37. Shan J, Zhao W, Gu W (2009) Suppression of cancer cell growth by promoting cyclin D1 degradation. *Mol Cell* 36:469–476.
38. Diehl JA, Zindy F, Sherr CJ (1997) Inhibition of cyclin D1 phosphorylation on threonine-286 prevents its rapid degradation via the ubiquitin-proteasome pathway. *Genes Dev* 11:957–972.
39. Mukherji A, Janbandhu VC, Kumar V (2008) GSK-3 $\beta$ -dependent destabilization of cyclin D1 mediates replicational stress-induced arrest of cell cycle. *FEBS Lett* 582:1111–1116.
40. Bates S, Peters G (1995) Cyclin D1 as a cellular proto-oncogene. *Semin Cancer Biol* 6:73–82.
41. Harris AW, et al. (1995) Cyclin D1 as the putative bcl-1 oncogene. *Curr Top Microbiol Immunol* 194:347–353.
42. Glinsky GV, Berezovska O, Glinskii AB (2005) Microarray analysis identifies a death-from-cancer signature predicting therapy failure in patients with multiple types of cancer. *J Clin Invest* 115:1503–1521.
43. Lin Z, et al. (2015) Ubiquitin-specific protease 22 is a deubiquitinase of CCNB1. *Cell Discov* 1:15028.
44. Wang XD, et al. (2011) SUMO-modified nuclear cyclin D1 bypasses Ras-induced senescence. *Cell Death Differ* 18:304–314.
45. Day PJ, et al. (2009) Crystal structure of human CDK4 in complex with a D-type cyclin. *Proc Natl Acad Sci USA* 106:4166–4170.
46. Benzeno S, et al. (2006) Identification of mutations that disrupt phosphorylation-dependent nuclear export of cyclin D1. *Oncogene* 25:6291–6303.
47. Hinds PW, Dowdy SF, Eaton EN, Arnold A, Weinberg RA (1994) Function of a human cyclin gene as an oncogene. *Proc Natl Acad Sci USA* 91:709–713.
48. Danielsen JM, et al. (2011) Mass spectrometric analysis of lysine ubiquitylation reveals promiscuity at site level. *Mol Cell Proteomics* 10:M1110.003590.
49. Lin Z, et al. (2012) USP22 antagonizes p53 transcriptional activation by deubiquitinating Sirt1 to suppress cell apoptosis and is required for mouse embryonic development. *Mol Cell* 46:484–494.
50. Germain D, Russell A, Thompson A, Hendley J (2000) Ubiquitination of free cyclin D1 is independent of phosphorylation on threonine 286. *J Biol Chem* 275:12074–12079.
51. Zwijsen RM, Buckle RS, Hijmans EM, Loomans CJ, Bernards R (1998) Ligand-independent recruitment of steroid receptor coactivators to estrogen receptor by cyclin D1. *Genes Dev* 12:3488–3498.
52. Pestell RG (2013) New roles of cyclin D1. *Am J Pathol* 183:3–9.
53. Casimiro MC, et al. (2012) ChIP sequencing of cyclin D1 reveals a transcriptional role in chromosomal instability in mice. *J Clin Invest* 122:833–843.
54. Carey MF, Peterson CL, Smale ST (2009) Dignam and Roeder nuclear extract preparation. *Cold Spring Harb Protoc* 2009:pdb.prot5330.
55. Zhang XY, et al. (2005) Metastasis-associated protein 1 (MTA1) is an essential downstream effector of the c-MYC oncoprotein. *Proc Natl Acad Sci USA* 102:13968–13973.
56. Rush J, et al. (2005) Immunoaffinity profiling of tyrosine phosphorylation in cancer cells. *Nat Biotechnol* 23:94–101.
57. Stokes MP, et al. (2015) Complementary PTM profiling of drug response in human gastric carcinoma by immunoaffinity and IMAC methods with total proteome analysis. *Proteomes* 3:160–183.
58. Stokes MP, et al. (2012) PTMScan direct: Identification and quantification of peptides from critical signaling proteins by immunoaffinity enrichment coupled with LC-MS/MS. *Mol Cell Proteomics* 11:187–201.
59. Rappsilber J, Ishihama Y, Mann M (2003) Stop and go extraction tips for matrix-assisted laser desorption/ionization, nano-electrospray, and LC/MS sample pretreatment in proteomics. *Anal Chem* 75:663–670.
60. Olsen JV, et al. (2005) Parts per million mass accuracy on an orbitrap mass spectrometer via lock mass injection into a C-trap. *Mol Cell Proteomics* 4:2010–2021.
61. Eng JK, McCormack AL, Yates JR (1994) An approach to correlate tandem mass spectral data of peptides with amino acid sequences in a protein database. *J Am Soc Mass Spectrom* 5:976–989.
62. Lundgrén DH, Martínez H, Wright ME, Han DK (2009) Protein identification using Sorcerer 2 and SEQUEST. *Curr Protoc Bioinformatics* Chapter 13:Unit 13.13.
63. Sussman RT, Zhang XY, McMahon SB (2011) Enzymatic assays for assessing histone deubiquitylation activity. *Methods* 54:339–347.
64. Peck AR, et al. (2011) Loss of nuclear localized and tyrosine phosphorylated Stat5 in breast cancer predicts poor clinical outcome and increased risk of antiestrogen therapy failure. *J Clin Oncol* 29:2448–2458.
65. Peck AR, et al. (2016) Validation of tumor protein marker quantification by two independent automated immunofluorescence image analysis platforms. *Mod Pathol* 29:1143–1154.
66. Lin DI, et al. (2006) Phosphorylation-dependent ubiquitination of cyclin D1 by the SCF(FBX4- $\alpha$ Crystallin) complex. *Mol Cell* 24:355–366.
67. Gong Y, et al. (2014) Pan-cancer genetic analysis identifies PARK2 as a master regulator of G1/S cyclins. *Nat Genet* 46:588–594.
68. Ganiatsas S, Dow R, Thompson A, Schulman B, Germain D (2001) A splice variant of Skp2 is retained in the cytoplasm and fails to direct cyclin D1 ubiquitination in the uterine cancer cell line SK-UT. *Oncogene* 20:3641–3650.
69. Spruck C, et al. (2001) A CDK-independent function of mammalian Cks1: Targeting of SCF(Skp2) to the CDK inhibitor p27Kip1. *Mol Cell* 7:639–650.
70. Yu ZK, Gervais JL, Zhang H (1998) Human CUL-1 associates with the SKP1/SKP2 complex and regulates p21(CIP1/WAF1) and cyclin D proteins. *Proc Natl Acad Sci USA* 95:11324–11329.
71. Okabe H, et al. (2006) A critical role for FBXW8 and MAPK in cyclin D1 degradation and cancer cell proliferation. *PLoS One* 1:e128.